1

# Undrained cyclic shear characteristics and crushing behaviour of silica sand

Yang Wu[*1,2], Masayuki Hyodo[2a] and Noritaka Aramaki[3b]

[1]*School of Civil Engineering, Guangzhou University, Guangzhou 510006, China*
[2]*Graduate School of Sciences and Technology for Innovation, Yamaguchi University, Ube 755-8611, Japan*
[3]*Horonobe Research Institute for the Subsurface Environment, Northern Advancement Center for Science and Technology, Hokkaido 098-3221, Japan*

**Abstract.**  This paper presents an investigation of the liquefaction characteristics and particle crushing of isotropically consolidated silica sand specimens at a wide range of confining pressures varying from 0.1 MPa to 5 MPa during undrained cyclic shearing. Different failure patterns of silica sand specimens subjected to undrained cyclic loading were seen at low and high pressures. The sudden change points with regard to the increasing double amplitude of axial strain with cycle number were identified, regardless of confining pressure. A higher cyclic stress ratio caused the specimen to liquefy at a relatively smaller cycle number, conversely producing a larger relative breakage $B_r$. The rise in confining pressure also resulted in the increasing relative breakage. At a specific cyclic stress ratio, the relative breakage and plastic work increased with the rise in the cyclic loading. Less particle crushing and plastic work consumption was observed for tests terminated after one cyclic loading. Majority of the particle crushing was produced and majority of the plastic work was consumed after the specimen passed through the phase transformation point and until reaching the failure state. The large amount of particle crushing resulted from the high-level strain induced by particle transformation and rotation.

**Keywords:**  undrained cyclic test; liquefaction; particle crushing; relative density; cyclic stress ratio

## 1. Introduction

Laboratory investigations have been extensively conduced to gain a better understanding of the monotonic and cyclic response of sand using simple and triaxial shear tests in undrained conditions (Seed and Lee 1966, Castro 1975, Ishihara *et al.* 1975, Castro and Poulos 1977, Mohamad and Dobry 1986, Vaid and Thomas 1995, Hyodo *et al.* 1996, 1998, Dash and Sitharam 2001, Vaid *et al.* 2001, Mao and Fahey 2003, Qadimi and Coop 2007, Murthy *et al.* 2007, Flora *et al.* 2012, Cabalar *et al.* 2013, Salem *et al.* 2013, Duman *et al.*2014, Cabalar 2016). The strength correspondence of sand between the monotonic and cyclic tests has been examined by many researchers (Hyodo *et al.* 1998, Mao and Fahey 2003, Porcino *et al.* 2008). In 1996 during the Great Hanshin earthquake, significant particle breakage failure of weak-grained soil in the Kobe Port Island area was noticed after the seismic loading. It remains uncertain whether particle breakage of hard-grained sand subjected to cyclic loading in high-pressure regions occurs and how it affects the liquefaction behaviour. However, the majority of previous dynamic research on sand was performed in low-pressure regions. The liquefaction resistance strength characteristics of granular materials at high pressure remain unclear. For example, the methane hydrate bearing sediment, expected to be a potential new energy resource, exists in the marine continental margins under a specific low temperature and high-pressure condition. Static and dynamic mechanical characteristics of methane hydrate bearing sediment are of great interest for the implementation of offshore gas extraction tests and in consideration of earthquakes (Hyodo *et al.* 2005, 2017a).

Particle crushing greatly affects the shear strength and deformation sand in drained triaxial shear test (Marsal 1973, Lade *et al.* 1996, Wu *et al.* 2013, Yoshimoto *et al.* 2016). The crushing behaviour of granular material subjected to cyclic loading in drained conditions has attracted the attentions of several researchers in recent decades. Donohue *et al.* (2009) noted that the degree of particle crushing of carbonate sand was affected by the stress level, cyclic stress ratio, and creep and was closely associated with the volumetric change. López-Querol and Coop (2012) observed that no obvious particle breakage of loose Dogs Bay sand at a maximum confining pressure of 500 kPa and that the volumetric strain approached its equilibrium as cycle loading continued.

Very few experimental investigations have been implemented to clarify the influential parameters affecting the crushing behaviour of sand subjected to undrained cyclic loading. In particular, the dynamic characteristic of hard-grained sand at high pressures is not fully understood, and the effect of particle breakage caused by cyclic loading is often neglected. Hyodo *et al.* (2000, 2002, 2017b) performed undrained monotonic and cyclic triaxial tests on hard-grained silica sand at medium-dense states in non-crushing and crushing regions and compared the particle

---

∗Corresponding author, Ph.D.
  E-mail: yangwuuu0226@hotmail.com
[a]Professor
[b]Ph.D.

crushing of isotropically and anisotropically consolidated specimens. The initial drained shear stress ratio had minimal effects on the degree of particle breakage at steady state. Agustian and Goto (2008) observed substantial particle breakage of scoria specimens after undrained cyclic loading. Orense *et al.* (2015) tested the pumice sand, a crushable volcanic soil, and noted that the extent of particle crushing remarkably increased as the failure state was reached. These studies contributed to the understanding of the development of particle crushing of cycled specimens in undrained conditions. However, the degree of particle crushing was quantified by the surface area $S$ (Miura and Toyotoshi 1975) and the breakage index $B_g$ (Marsal 1973), which were not widely employed to evaluate the overall change in the grain size distribution curve.

This paper presents an experimental investigation on the undrained cyclic characteristics of silica sand at medium-dense state at low and high confining pressures through a triaxial shear test. This study intends to investigate the effects of confining pressure and cyclic stress ratio on the undrained cyclic response and particle crushing behaviour. The dependence of the liquefaction resistance strength on the particle crushing is also clarified. The evolution of particle crushing and plastic work of silica sand during the entire cyclic shearing process is thoroughly investigated. In one undrained cyclic test, the grain size distribution curve of a tested specimen is determined, and the degree of particle crushing is assessed after several distinctive stages, such as after one cycle, at the phase transformation (PT) point, and at the failure state point. The degree of particle crushing is re-quantified using the rational parameter $B_r$, proposed previously (Einav 2007), to facilitate the comparison with published data in the literature. Besides, the test results of Aio sand with initial void ratio of 0.657 at dense state in undrained cyclic test had been published by authors (Hyodo *et al.* 2002). Thus, this study also makes the comparison study on undrained cyclic characteristics of Aio sands at different densities possible. The effect of the density on the relationship between the particle crushing and plastic work in undrained conditions is examined for silica sand in high-pressure regions.

## 2. Tested materials and conditions

Sand was obtained from the Aio beach south of the Yamaguchi prefecture in the Chugoku region of Japan. Fig. 1 shows the grain size distribution curve of Aio sand, which is a well-graded silica sand that contains many sharp-edged grains. Its major components are quartz and feldspar. It has a specific gravity $G_s =2.64$ and a uniform coefficient $U_c=2.74$, along with minimum ($e_{min}$) and maximum ($e_{max}$) void ratios of 0.582 and 0.958, respectively.

The tests were conducted using a high-pressure triaxial testing apparatus devised at Yamaguchi University. This testing apparatus can provide a maximum cell pressure up to 50 MPa and a wide range of cyclic loading frequencies from 0.001 Hz to 100 Hz. Cylindrical specimens, 50 mm in diameter and 100 mm in height, were prepared using air pluviation methods to attain the initial void ratio of 0.760 at medium-dense state and an initial density $\rho_d$=1590 kg/cm$^3$.
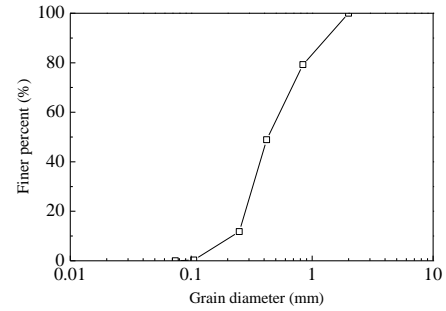


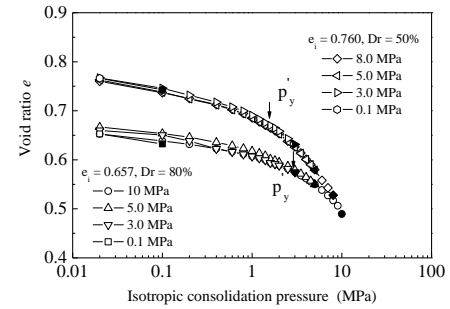Fig. 1 Grain size distribution curve of Aio sand



Fig. 2 Isotropic compression curves of Aio sand with two initial void ratios of 0.760 and 0.657 (Hyodo *et al.* 2017b)

The saturation process was accomplished until the Skempton's B value was greater than 0.95. The specimens were isotropically consolidated to different effective mean stresses of 0.1 MPa, 3 MPa, and 5 MPa. Fig. 2 presents the plot of the void ratio against the isotropic compression pressure of the medium-dense with initial void ratio of 0.760 and dense Aio sands with initial void ratio of 0.657, terminated at different compression pressures. The applied pressures were less than, approximately equal to, and beyond the yield stress $p_y'$ of Aio sand ( $p_y'$= 2 MPa for the medium-dense state, 3 MPa for the dense state) determined from the isotropic compression test. A large amount of particle crushing commenced when the applied confining pressure exceeded the corresponding yield stress $p_y'$. The cyclic loading was axially conducted by uniform sinusoidal cycles on specimens under stress controlled at different cyclic stress ratios (CSR) $\sigma_d/2\sigma_c'$ with a frequency of 0.05 Hz. Herein, the imposed cyclic stress ratio was defined as the ratio of the deviatoric stress $\sigma_d$ to the confining pressure $\sigma_c'$ . The axial strain, axial displacement, cell pressure, and excess pore water pressure were automatically recorded via a computer.

A sieving analysis test was performed after each undrained cyclic loading test, and the final grading distribution curve was determined. The grain size distribution curve of granular material accompanied by particle breakage tended to vary in accordance with the fractal distribution. Therefore, the rational index of relative breakage $B_r$ proposed by (Einav 2007) was employed to quantify the amount of particle crushing in this study. The $B_r$=0 represents for the unbroken granular material and the $B_r$=1 means the complete granular material. The ultimate grading curve is expressed as $(d/d_M)^{3-\alpha}$, where d is the grain

diameter and $d_M$ is the maximum grain diameter. The fractal dimension $\alpha=2.6$ was adopted for natural sand (Coop *et al.* 2004). To thoroughly examine the evolution of particle crushing during the entire process of undrained cyclic loading, the tests are specially terminated after the first cycle, at the PT point, and at the failure state point under the same given experimental conditions of confining pressure $\sigma_c'$, relative density, and cyclic stress ratio $\sigma_d/2\sigma_c'$. The sieving analysis tests were also performed on the tested specimens terminated at different stages to quantify the degree of particle breakage.
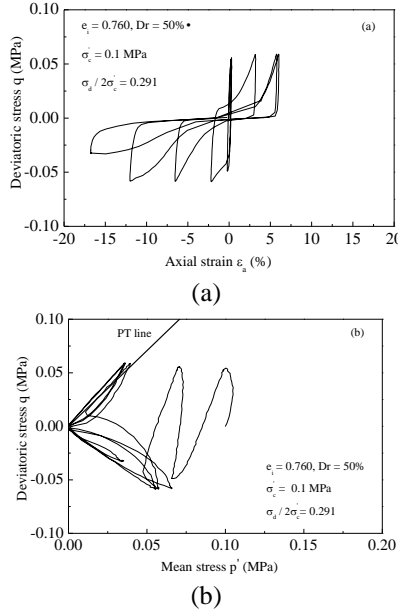


(a)

(b)

Fig. 3 Undrained cyclic response of Aio sand with initial void ratio of 0.760 at confining pressure of 0.1 MPa (a) Stress-strain curve and (b) Effective cyclic stress path
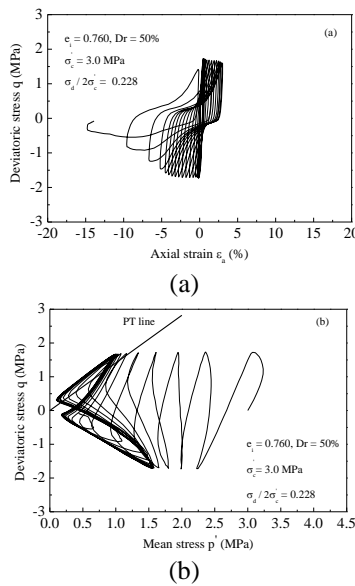


(a)

(b)

Fig. 4 Undrained cyclic response of loose Aio sand with initial void ratio of 0.760 at confining pressure of 3.0 MPa (a) Stress-strain curve and (b) Effective cyclic stress path
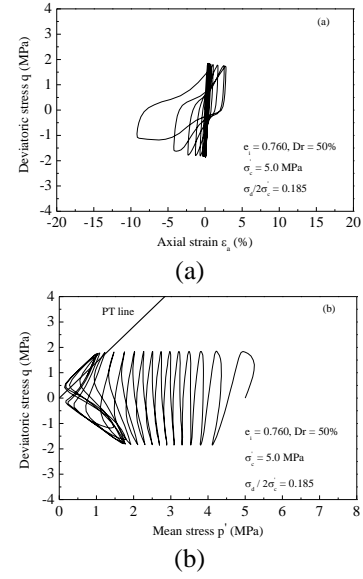


(a)

(b)

Fig. 5 Undrained cyclic response of loose Aio sand with initial void ratio of 0.760 at confining pressure of 5.0 MPa (a) Stress-strain curve and (b) Effective cyclic stress path

## 3. Undrained cyclic shear response

### 3.1 Stress-strain characteristics

Figs. 3(a) and 3(b) show the typical undrained cyclic response of Aio sand. The specimens are isotropically consolidated to a confining pressure of 0.1 MPa ($\sigma_c' < p_y' = 2$ MPa) and cycled at a cyclic stress ratio $\sigma_d/2\sigma_c'$ of 0.291. The effective mean stress quickly reduces when accompanied by the generation of the excess pore water pressure $u$ as the cyclic loading proceeds. Liquefaction failure occurs once the effective mean stress reduces to zero. A larger axial strain, triggered by the rapid build-up of the excess pore water pressure u, eventually causes the loose specimens to decrease in strength. An axial strain amplitude is produced in both the compression and extension sides in excess of 5%. In a previous study, Hyodo *et al.* (1998) noticed the similar results on loose Masado and Shirasu soils at the same level of confining pressure as the applied one in this investigation.

Figs. 4(a) and 4(b) present the stress-strain relationship and effective cyclic stress path of Aio sand at a confining pressure of 3 MPa ($\sigma_c' > p_y' = 2$ MPa). The axial stain is slowly developed at the initial stages, and a larger axial strain is produced in the extension side at the failure state owing to the anisotropic characteristics of granular material, as shown in Fig. 4(a). The effective mean stress does not reach zero at the failure state even if the specimen experiences a larger number of cycles. Another failure pattern "cyclic mobility" was observed for loose specimens in high-pressure regions. This cyclic failure criterion is defined as the condition when a double amplitude (DA) of axial strain $\varepsilon_{DA}=5\%$ is reached. The excessive deformation originated from the progressive stiffness degradation owing to the generation of excess pore water pressure.

Aio sand specimens exhibited a similar cyclic mobility behaviour at a confining pressure of 5 MPa ($\sigma_c^{'} > p_y^{'} = 2$ MPa), as shown in Fig. 5. The double amplitude of axial strain $\varepsilon_{DA}$ at two relative densities of specimens continually accumulates as the number of cycles increases until finally reaching an excess of 5%. Although the axial strain is simultaneously developed in both the compression and extension sides, a relatively larger amplitude of the axial strain is observed in the extension side.

### 3.2 Evolution of excess pore water pressure and double amplitude of axial strain

In undrained cyclic loading, the excess pore water pressure $u$ and double amplitude of axial strain $\varepsilon_{DA}$ are two major quantities affecting the cyclic and crushing behaviours at a wide range of confining pressures. Therefore, another series of undrained cyclic triaxial shear tests were performed at a similar cyclic stress ratio $\sigma_d/2\sigma_c^{'}$, but with variable confining pressures. The normalized pore pressure ratio $r_u = u/\sigma_c^{'}$ is the ratio of the excess pore water pressure u to the applied confining pressure $\sigma_c^{'}$. Fig. 6 presents the plot of the normalized pore pressure ratio $r_u$ against the number of cycles for silica sands at low and high confining pressures. The curves exhibit similar tendencies at each confining pressure. The normalized pore pressure ratio $r_u$ of silica sand at a confining pressure of 0.1 MPa dramatically increases after three cycles (N=3), and it finally reaching a value of one when the excess pore water pressure u is identical to the initial compression pressure. The sudden change point in the curve, with regard to the normalized pore pressure ratio $r_u$, is closely associated with the onset of liquefaction of specimens. The sudden change point was also noticed in other investigations (Konstadinou and Georgiannou 2013, Salem *et al.* 2013). No obvious sudden change points are observed in the rest curves, but these curves demonstrate that the increasing rate of the normalized pore pressure ratio with the cycle number N gradually accelerates.

Fig. 7 shows the double amplitude of axial strain $\varepsilon_{DA}$ plotted against the number of cycles N of tested specimens at variable confining pressures. The experimental results show that almost no remarkable change in the axial strain is observed before a critical cycle number N, and a rapid rise in the axial strain commences after that critical cycle number N, regardless of the relative density and confining pressure. Aio sand experiences a rapid rise in double amplitude of axial strain after the cycle number N=3 at a confining pressure 0.1 MPa. The axial strain of is difficult to be produced when the confining pressure is increased to 3 MPa and 5 MPa.

The rapid rise in the excess pore water pressure u occurs at an earlier cycle number than the appearance of the sudden change point on the curve for the double amplitude of axial strain. The generation of excess pore water pressure $u$ reduces the effective mean stress and further gives rise to the instability of the sand specimens as the cyclic loading progresses.

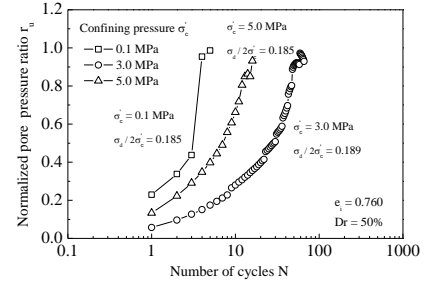### 3.3 Liquefaction resistance strength curve



Fig. 6 Normalized pore pressure ratio plotted against the number of cycle *N*
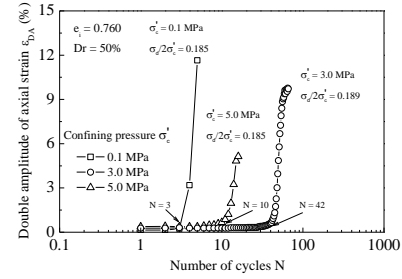


Fig. 7 Double amplitude of axial strain plotted against the number of cycles *N*
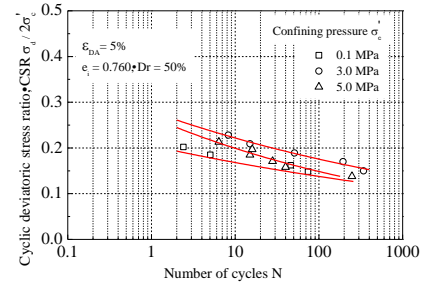


Fig. 8 Liquefaction resistance strength of Aio sand with initial void ratio of 0.760
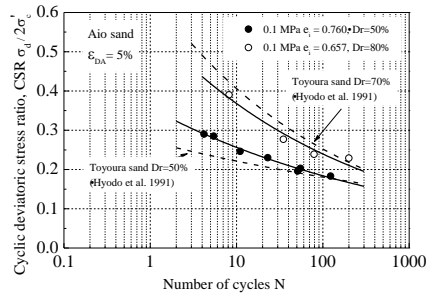


Fig. 9 Effect of relative density on the liquefaction resistance strength at confining pressure of 0.1 MPa (Hyodo *et al.* 2017b)

Fig. 8 presents the liquefaction resistance strength plotted against the cycle number of Aio sand at low and high confining pressures. The liquefaction resistance strength characteristics of the specimens is examined in the non-crushing ($\sigma_c^{'} < p_y^{'}$) and crushing ($\sigma_c^{'} \geq p_y^{'}$) regions. The liquefaction resistance strength is defined as the ratio of the applied cyclic stress to the confining pressure, $\sigma_d/2\sigma_c^{'}$. The cyclic resistance strength of silica sand initially increases at confining pressures varying from 0.1 MPa to 3 MPa and

decreases as the confining pressure increases to 5 MPa. The confining pressure dependence of the specimen is not clear. This result corresponds to the observation of liquefaction failure of specimens at relatively smaller cycle numbers and a low confining pressure of 0.1 MPa, as shown in Fig. 7. However, it was demonstrated that the cyclic resistance strength of dense Aio sand tended to decrease as the applied confining pressure $\sigma_c'$ was increased (Hyodo *et al.* 2002). Similar results on other types of sand have been reported by (Castro and Poulos 1977, Hyodo *et al.* 1998, Salem *et al.* 2013). Particle crushing has been identified as the major contributor to this tendency.

Fig. 9 illustrates the effect of the relative density on the liquefaction resistance strength at a low confining pressure of 0.1 MPa. The liquefaction resistance strength of Toyoura sand at two relative densities of 50% and 70% are added for a comparison (Hyodo *et al.* 1991). The rise in the density increased the liquefaction resistance strength of Aio sand. A similar pattern was observed for Toyoura sand at the same level of confining pressure. The extent of the liquefaction resistance strength enhancement is largely determined by the inherent characteristics and internal structure of the sand.

## 4. Particle crushing in undrained cyclic tests

### 4.1 Effect of cyclic stress ratio on particle crushing

A series of undrained cyclic triaxial tests was performed on Aio sands at different cyclic stress ratios to examine its effect on the degree of particle breakage. Fig. 10 shows that the relative breakage $B_r$ plotted against the cyclic stress ratio. Particle crushing is also assessed in isotropic compression tests to differentiate the particle damage solely by cyclic loading. Thus, the relative breakage Br is a non-zero value at $\sigma_d/2\sigma_c'=0$. It is interesting here to note that the particle crushing indeed occurs after a number of cyclic loadings in undrained conditions; although, the effective mean stress continually decreases. This is attributed to high-level strain developed as the cyclic loading progresses. The relative breakage tends to increases with the level of cyclic stress ratio. Yoshimoto *et al.* (2014) noticed significant particle breakage after cyclic shear increased with higher confining pressures and explained that breakage was caused more by the shear stress rather than the normal stress. The sand crushing is expected to occur under cyclic loading such as earthquake or structure vibration (Yi *et al.* 2001, 2012a, 2012b).

Fig. 11 illustrates the influence of the confining pressure $\sigma_c'$ on the liquefaction resistance strength and relative breakage $B_r$ of Aio sand. Therefore, only experimental data indicating marked breakage at confining pressures $\sigma_c'$ of 3 MPa and 5 MPa are shown. For Aio sand, the specific cycle number N in accordance with liquefaction varies from less than 6 to around 400. The corresponding relative breakage $B_r$ determined after the liquefaction state is also plotted against the specific cycle number N at different cyclic stress ratios. A higher cyclic stress ratio $\sigma_d/2\sigma_c'$ causes the specimen to liquefy at a relatively smaller cycle number, conversely producing a larger relative breakage $B_r$. A
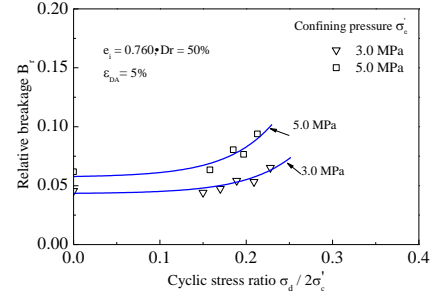


Fig. 10 Relative breakage plotted against the cyclic stress ratio of loose Aio sand with initial void ratio of 0.760 (Hyodo *et al.* 2017b)
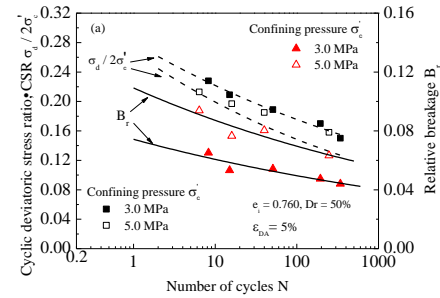


Fig. 11 The cyclic stress ratio and relative breakage plotted against the number of cycle *N* in undrained cyclic test on Aio sand with initial void ratio of 0.760
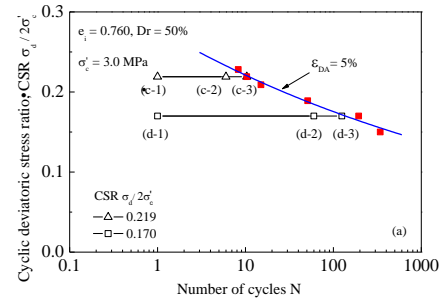


Fig. 12 Stress path at different cyclic stress ratios in undrained cyclic test

contrary influence of the confining pressure on variations in the liquefaction resistance strength and degree of particle crushing was noticed. An increasing confining pressure reduces the liquefaction resistance strength, but improves the relative breakage. As the cycle number progresses, both the liquefaction resistance strength curve and the curve describing the variation in the relative breakage gradually become flatter.

### 4.2 Evolutions of particle crushing and plastic work in undrained cyclic tests

To investigate the evolutions of particle crushing and plastic work in undrained cyclic loading at a given cyclic stress ratio, the tests were terminated at three distinctive stages, including after the first cycle, at the PT point, and at the failure state point when the double amplitude of axial strain $\varepsilon_{DA}$= 5% is reached. Fig. 12 shows the designated stress paths of Aio sands at two cyclic stress ratios. The
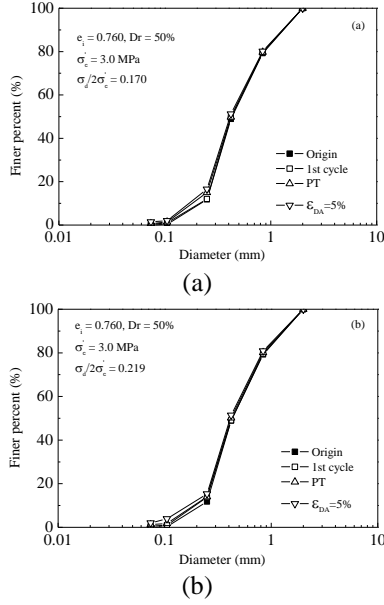
Fig. 13 GSD curve of Aio sand at different stages in undrained cyclic test with different initial deviatoric stress ratios (a) at cyclic stress ratio of 0.170 and (b) at cyclic stress ratio of 0.219
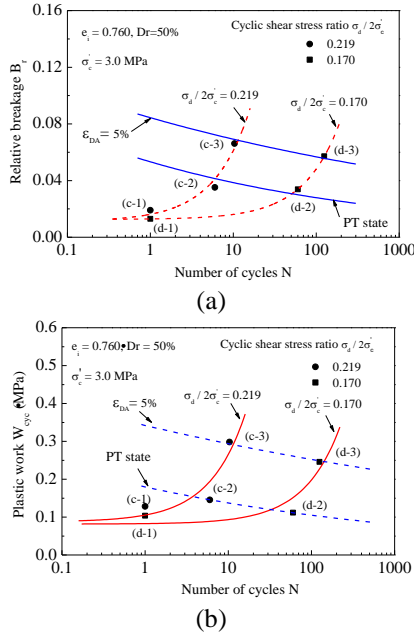


Fig. 14 The evolutions of particle crushing and plastic work at different cyclic stress ratios in undrained cyclic test ($e_i$ = 0.760, 3 MPa) (a) relative density versus the number of cycle and (b) plastic work versus the number of cycle
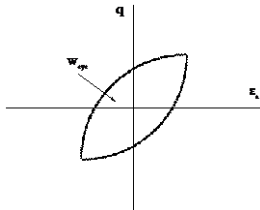


Fig. 15 Determination method of the plastic work in undrained cyclic test

cycle number N corresponding to the PT point and failure state point increase with the decreasing cyclic stress ratio. Figs. 13(a) and 13(b) show the variation in the grain size distribution curves of Aio sand at different cyclic stress ratios before testing and after several distinctive stages. An obvious change in the grading curve from tests terminated after the different stages is observed. A gradual shift of the grading curves is confirmed, accompanied by the stress paths proceeding from one cycle to the PT point and finally the failure state.

Figs. 14(a) and 14(b) show the evolution of the relative breakage $B_r$ and plastic work $W_{cyc}$ of Aio sand with increasing cycle number N at two cyclic stress ratios and a confining pressure $\sigma'_c$=3 MPa. The plastic work $W_{cyc}$ of specimens during cyclic loading can be calculated using a simple method as the area of the stress-strain hysteresis loop shown in Fig. 15. The separate points from (c-1) to (d-3) in Figs. 14(a) and 14(b) correspond to those in Fig. 12. Contour lines representing the PT state point and the failure state point are also drawn, intersecting with the curve expressing the evolution of the relative breakage. Moreover, the contour lines exhibit an opposite variable tendency to the relative breakage and plastic work evolution curves with the level of cycle number N. Fig. 14 presents the relationship between the plastic work and the number of cycles.

At a specific cyclic stress ratio, the relative breakage and plastic work increase as the cycle number N progresses. The particle breakage and plastic work evolution curves become steeper with increasing cycle number. No remarkable amount of particle crushing and plastic work occurs after the first cycle loading. A slight difference in the relative breakage and plastic work is observed after the first cycle at two different cyclic stress ratios. Only a small amount of particle crushing and plastic work is observed after the PT point ($\sigma_d/2\sigma'_c$=0.219, N=6; $\sigma_d/2\sigma'_c$=0.170, N=60). A large amount of particle crushing occurred and a large amount of plastic work was consumed after passing through the PT point until reaching the failure state point ($\sigma_d/2\sigma'_c$=0.219, N=10.4; $\sigma_d/2\sigma'_c$=0.170, N=135). This results from the high-level axial strain induced by the particle rotation and translation. The relative breakage and plastic work at three distinctive stages are all higher at a cyclic stress ratio of $\sigma_d/2\sigma'_c$=0.219. It is inferred that the particle breakage evolution curve becomes flatter as the cyclic stress ratio decreases.

### 4.3 Relationship between the particle breakage and plastic work in undrained condition

The test results revealed that tendencies of relative breakage and plastic work similarly varied with the level of cycle number. Besides, the existence of well relationship between relative breakage and plastic work for sand in drained condition had been pointed out in previous studies (Lade *et al.* 1996, Daouadji *et al.* 2001). It is necessary to investigate the relationship between these two variables in undrained condition.

The relative breakage is plotted against the plastic work for Aio sand at medium-dense state in Fig. 16. The test data for Aio sand at dense state was also added for a
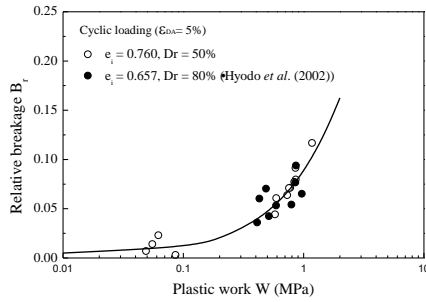
Fig. 16 The relationship between the relative breakage and plastic work of Aio sand at two initial void ratios in undrained cyclic loading test

comparison study (Hyodo *et al.* 2002). A unique correlation between the relative breakage $B_r$ and plastic work $W_p$ could be obtained, regardless of confining pressure and termination point. This relation can also be described using the expression of $B_r = W_p/(a+W_p)$ (Lade *et al.* 1996). a is a material constant and takes the value of 10.3 MPa. The influence of the initial density on the relationship between the plastic work and relative breakage for Aio sand is minimal in undrained cyclic loading test. It is attributed to relatively smaller total amount of particle crushing in undrained cyclic loading test.

## 5. Conclusions

A series of undrained cyclic triaxial tests was performed on Aio sand to examine the effects of confining pressure and cyclic stress ratio on its undrained cyclic response and crushing behaviour. To investigate the evolutions of particle crushing and plastic work in undrained cyclic triaxial tests, the cyclic triaxial tests were specifically terminated at several distinctive stages, such as after one cycle, at the PT point, and at the liquefaction state (failure state) point. Subsequently, a sieving analysis test was conducted on each cycled specimen, and the particle crushing was quantified by the relative breakage index $B_r$. The correlation between the particle breakage and plastic work for Aio sand at different initial void ratios are examined in cyclic loadings. Based on the results presented in this study, the major conclusions can be drawn as follows.

1. Two representative failure patterns of Aio sand, subjected to undrained cyclic loading at a wide range of confining pressures, are identified. The liquefaction failure of silica sand occurs at a low confining pressure of 0.1 MPa. The cyclic mobility response of silica sand at a high confining pressure of 5 MPa is observed.

2. The normalized pore pressure ratio $r_u$ increases, and its rate of increase gradually accelerates as the cyclic loading progresses. A sudden change point on the curve with regard to the double amplitude of axial strain is identified for Aio sand, regardless of the confining pressure. The axial strain amplitude dramatically increases after a sudden change point and finally exceeds a 5% amplitude.

3. At confining pressures of 3 MPa and 5 MPa, a contrary influence of the confining pressure on the variations in the liquefaction resistance strength curve and

the particle breakage evolution curve is noticed. A higher confining pressure reduces the liquefaction resistance strength and intensifies the degree of particle breakage. Besides, a higher cyclic stress ratio causes the specimen to liquefy at a relatively smaller cycle number, conversely producing a larger relative breakage $B_r$.

4. At a given cyclic stress ratio $\sigma_d/2\sigma_c'$, confining pressure, and relative density, the relative breakage and plastic work increase as the cycle number N progresses. Less particle crushing and plastic work $W_{cvc}$ is observed after only one cyclic loading at two cyclic stress ratios. Only a small amount of particle crushing and plastic work is observed as the specimen is cycled to the PT point. A large amount of the relative breakage and plastic is noted when the specimen passes through the PT point and until reaching the liquefaction state point. This is due to the high-level axial strain induced by the particle transformation and rotation.

5. A unique correlation between the relative breakage and plastic work could be obtained, regardless of confining pressures and termination points. The influence of the initial density on the relationship between the relative breakage and plastic work for Aio sand is minimal in undrained cyclic loading test.

## References

Agustian, Y. and Goto, S. (2008), "Undrained cyclic shear behaviour of reconstituted scoria deposit", *Soils Found.*, **48**(6), 851-857.

Cabalar, A.F. (2016), "Cyclic behavior of various sands and structural materials interfaces", *Geomech. Eng.*, **10**(1), 1-19.

Cabalar, A.F., Dulundu, K. and Tuncay, K. (2013), "Strength of various sands in triaxial and cyclic direct shear tests", *Eng. Geol.*, **156**, 92-102.

Castro, G. (1975), "Liquefaction and cyclic mobility of saturated sands", *J. Geotech. Eng.*, **101**(6), 551-569.

Castro, G. and Poulos, S.J. (1977), "Factors affecting liquefaction and cyclic mobility", *J. Geotech. Eng.*, **103**(6), 501-506.

Coop, M.R., Sorensen, K.K., Freitas, T.B. and Georgoutsos, G. (2004), "Particle breakage during shearing of a carbonate sand", *Géotechnique*, **54**(3), 157-163.

Daouadji, A., Hicher, P.Y. and Rahma, A. (2001), "Elastoplastic model for granular materials taking into account grain breakage", *Eur. J. Mech. A/Solids*, **20**(1), 113-137.

Dash, H.K. and Sitharam, T.G. (2011), "Cyclic liquefaction and pore pressure response of sand-silt mixtures", *Geomech. Eng.*, **3**(2), 83-108.

Donohue, S., O'Sullivan, C. and Long, M. (2009), "Particle breakage during cyclic triaxial loading of a carbonate sand", *Géotechnique*, **59**(5), 477-482.

Duman, E.S., Ikizler, S.B., Angin, Z. and Demir, G. (2014), "Assessment of liquefaction potential of the Erzincan, eastern

Turkey", *Geomech. Eng.*, **7**(6), 589-612.

Einav, I. (2007), "Breakage mechanics-part I: Theory", *J. Mech. Phys. Solids*, **55**(6), 1274-1297.

Flora, A., Lirer, S. and Silvestri, F. (2012), "Undrained cyclic resistance of undisturbed gravelly soils", *Soil Dyn. Earthq. Eng.*, **43**, 366-379.

Hyodo, M., Aramaki, N., Itoh, M. and Hyde, A.F.L. (1996), "Cyclic strength and deformation of crushable carbonate sand", *Soil Dyn. Earthq. Eng.*, **15**(5), 331-336.

Hyodo, M., Hyde, A.F.L. and Aramaki, N. (1998), "Liquefaction of crushable soils", *Géotechnique*, **48**(4), 527-543.

Hyodo, M., Hyde, A.F.L., Aramaki, N. and Nakata, Y. (2002), "Undrained monotonic and cyclic shear behaviour of sand under low and high confining stresses", *Soils Found.*, **42**(3), 63-76.

Hyodo, M., Murata, H., Yasufuku, N. and Fuji, T. (1991), "Undrained cyclic shear strength and residual shear strain of saturated sand by cyclic triaxial tests", *Soils Found.*, **31**(3), 60-76.

Hyodo, M., Nakata, Y., Aramaki, N., Hyde, A.F.L. and Inoue, S. (2000), "Liquefaction and particle crushing of soil", *Proceedings of 12th World Conference on Earthquake Engineering*, Auckland, New Zealand, January.

Hyodo, M., Nakata, Y., Yoshimoto, N. and Ebinuma, T. (2005), "Basic research on the mechanical behavior of methane hydrate-sediments mixture", *Soils Found.*, **45**(1), 75-85.

Hyodo, M., Wu, Y., Aramaki, N. and Nakata, Y. (2017b) "Undrained monotonic and cyclic shear response and particle crushing of silica sand at low and high pressures", *Can. Geotech. J.*, **54**(2), 204-215.

Hyodo, M., Wu, Y., Kajiyama, S., Yoshimoto, N. and Nakata, Y. (2017a) "Effect of fines on the compression behaviour of poorly graded silica sand", *Geomech. Eng.*, **12**(1), 127-138.

Ishihara, K., Tatsuoka, F. and Yasuda, S. (1975), "Undrained deformation and liquefaction of sand under cyclic stresses", *Soils Found.*, **15**(1), 29-44.

Konstadinou, M. and Georgiannou, V.N. (2013), "Cyclic Behaviour of loose anisotropically consolidated Ottawa sand under undrained torsional loading", *Geotechnique*, **63**(13), 1144-1158.

Lade, P.V. and Yamamuro, J.A. (1997), "Effects of nonplastic fines on static liquefaction of sands", *Can. Geotech. J.*, **34**(6), 918-928.

Lade, P.V., Yamamuro, J.A. and Bopp, P.A. (1996), "Significance of particle crushing in granular materials", *J. Geotech. Geoenviron. Eng.*, **122**(4), 309-316.

López-Querol, S. and Coop, M.R. (2012), "Drained cyclic behaviour of loose Dogs Bay sand", *Géotechnique*, **62**(4), 281-289.

Mao, X. and Fahey, M. (2003), "Behaviour of calcareous soils in undrained cyclic simple shear", *Géotechnique*, **53**(8), 715-727.

Marsal, R.J. (1967), "Large-scale testing of rockfill materials", *J. Soil Mech. Found. Div.*, **93**(2), 27-43.

Marsal, R.J. (1973), *Mechanical Properties of Rockfill*, In *Embankment Dam Engineering*.

Miura, N. and Toyotoshi, Y. (1975), "Effect of water on the behavior of a quartz-rich sand under high stresses", *Soils Found.*, **15**(4), 23-34.

Mohamad, R. and Dobry, R. (1986), "Undrained monotonic and cyclic triaxial strength of sand", *J. Geotech. Eng.*, **112**(10), 941-958.

Murthy, T.G., Loukidis, D., Carraro, J.A.H., Prezzi, M. and Salgado, R. (2007), "Undrained monotonic response of clean and silty sands", *Géotechnique*, **57**(3), 273-288.

Nakata, Y., Hyodo, M., Hyde, A.F.L., Kato, Y. and Murata, H. (2001), "Microscopic particle crushing of sand subjected to high pressure one-dimensional compression", *Soils Found.*, **41**(1), 69-82.

Porcino, D., Caridi, G. and Ghionna, V.N. (2008), "Undrained monotonic and cyclic simple shear behaviour of carbonate sand", *Géotechnique*, **58**(8), 635-644.

Qadimi, A. and Coop, M.R. (2007), "The undrained cyclic behaviour of a carbonate sand", *Géotechnique*, **57**(9), 739-750.

Salem, M., Elmamlouk, H. and Agaiby, S. (2013), "Static and cyclic behavior of north coast calcareous sand in Egypt", *Soil Dyn. Earthq. Eng.*, **55**, 83-91.

Seed, H.B. and Lee, K.L. (1966), "Liquefaction of saturated sands during cyclic loading", *J. Soil Mech. Found. Div.*, **92**(6), 105-134.

Vaid, Y.P. and Thomas, J. (1995), "Liquefaction and postliquefaction behaviour of sand", *J. Geotech. Eng.*, **121**(2), 163-173.

Vaid, Y.P., Stedman, J.D. and Sivathayalan, S. (2001), "Confining stress and static shear effects in cyclic liquefaction", *Can. Geotech. J.*, **38**(3), 580-591.

Wu, Y., Yamamoto, H. and Yao, Y.P. (2013), "Numerical study on bearing behavior of pile considering sand particle crushing", *Geomech. Eng.*, **5**(3), 241-261.

Yasufuku, N., Murata, H. and Hyodo, M. (1991), "Yield characteristics of anisotropically consolidated sand under low and high stresses", *Soils Found.*, **31**(1), 95-109.

Yi, T.H., Li, H.N. and Gu, M. (2011), "Characterization and extraction of global positioning system multipath signals using an improved particle-filtering algorithm", *Meas. Sci. Technol.*, **22**(7), 075101.

Yi, T.H., Li, H.N. and Gu, M. (2012b). "Effect of different construction materials on propagation of GPS monitoring signals", *Measurement*, **45**(5), 1126-1139.

Yi, T. H., Li, H. N. and Zhao, X.Y. (2012a), "Noise smoothing for structural vibration test signals using an improved wavelet thresholding technique", *Sensors*, **12**(8), 11205-11220.

Yoshimoto, N., Orense, R.P., Hyodo, M. and Nakata, Y. (2014), "Dynamic behavior of granulated coal ash during earthquakes", *J. Geotech. Geoenviron. Eng.*, **140**(2), 04013002.

Yoshimoto, N., Wu, Y., Hyodo, M. and Nakata, Y. (2016), "Effect of relative density on the shear behaviour of granulated coal ash", *Geomech. Eng.*, **10**(2), 207-224.

*CC*